

A MAV That Flies Like an Airplane and Hovers Like a Helicopter

William E. Green and Paul Y. Oh*
Drexel University, Philadelphia, PA
[weg22,paul.yu.oh]@drexel.edu

Abstract

Near-Earth environments, such as forests, caves, tunnels, and urban structures make reconnaissance, surveillance and search-and-rescue missions difficult and dangerous to accomplish. Micro-Air-Vehicles (MAVs), equipped with wireless cameras, can assist in such missions by providing real-time situational awareness. This paper describes an additional flight modality enabling fixed-wing MAVs to supplement existing endurance superiority with hovering capabilities. This secondary flight mode can also be used to avoid imminent collisions by quickly transitioning from cruise to hover flight. A sensor suite which will allow for autonomous hovering by regulating the aircraft's yaw, pitch and roll angles is also described.

1 Introduction

Micro-Air-Vehicles (MAVs) are small, lightweight aircraft used to perform reconnaissance, surveillance, and inspection missions. Such missions can occur in a variety of environments. For example, lengthy recon flights across a desert or hovering above a foreign building to collect target information. Oftentimes the specifics of the mission dictate the MAV platform configuration. If vertical takeoff or hovering is required, then rotary-wing aircraft, such as a quad-rotors [8] or ducted fans [3], are most optimal. However, if endurance is a priority, then a fixed-wing body type will most likely be selected.

We are currently designing a MAV platform that offers both the endurance superiority of a fixed-wing aircraft coupled with the hovering capabilities of rotary-wing vehicles. This is achieved through a flight maneuver known as prop-hanging. During a prop-hang, the longitudinal axis of the fuselage remains vertical

*This material is based upon work supported by the National Science Foundation under Grant No. 0347430. Any opinions, findings, and conclusions or recommendations expressed in this material are those of the author(s) and do not necessarily reflect the views of the National Science Foundation. Pages: <http://www.pages.drexel.edu/~weg22/research.html>



Figure 1: Our MAV prototype combines the endurance of fixed-wing platforms with the hovering capabilities of rotary-wing aircraft. This allows it to carry out missions in cluttered terrain such as forests.

while the weight of the aircraft is supported by the thrust from the propeller (see Figure 1). This requires unconventionally large thrust-to-weight ratios ($T/W > 1$). The net result is a vehicle which primarily translates but can perform high angle-of-attack (AOA) maneuvers as a secondary flight modality.

The primary interest of the authors is to develop a backpackable, low-cost, high-endurance platform and sensor suite allowing autonomous flight in near-Earth environments. The classification of near-Earth describes low-altitude areas which are rugged and richly populated with obstacles. Examples include forests, caves, tunnels and urban structures. Flying in such environments presents unconventional challenges such as poor GPS signals and degraded communications. Furthermore, cluttered terrain demands a platform which is small and can fly safely and slowly (< 5 m/s). Other fixed-wing MAVs, such as Aerovironment's Black Widow [5], fly too fast for this environment. Rotary-wing aircraft can hover but are restricted by endurance capabilities. A blimp's lifting capacity is proportional to its volume and thus,

have too much inertia to effectively maneuver in near-Earth environments. Micromechanical flying insects are a promising platform, but are currently limited to tethered flight [4]. The net effect is that few high-endurance platforms exist which are highly maneuverable in near-Earth environments. As such, the secondary flight modality was incorporated into the fixed-wing design to combine both endurance and maneuverability.

Using a conventional fixed-wing MAV (i.e. without hovering capabilities), the authors were the first to demonstrate autonomous landing and collision avoidance in urban structures [6] [10]. An optic flow sensor was used to gain information on incoming collisions and altitude while the control system mimicked insect flight stratagems. One instance where optic flow will fail, however, is when an approaching obstacle remains aligned with the sensor's optical axis. In this case, the additional flight modality can be utilized in conjunction with a simple proximity sensor to detect and avoid the obstacle by a quick transition from cruise to hover. This paper illustrates the usefulness of a hovering, fixed-wing aircraft for flight in cluttered terrain. Section 2 discusses fixed and rotary-wing thrust and endurance characteristics. Section 3 presents the governing equation of motion as well as model and flight data for the cruise-to-hover transition. This is followed by a section on future work and section 5 concludes by summarizing.

2 Fixed and Rotary-Wing Platforms

Fixed-wing aircraft are typically preferred for missions where endurance is a priority because the main lift component is provided by wings as opposed to electric motors. During forward flight, helicopters must balance the weight of the body with thrust from the main rotor thus, draining the power source quicker. The following analysis shows the thrust and endurance ratios for each of the two platform configurations.

2.1 Required Thrust

The overall endurance of each aircraft is dependent upon the amount of thrust required to sustain steady, level flight. In order to make a valid comparison between the required thrust for both fixed-wing and rotary-wing MAVs, the following assumptions are made

1. $W_{heli} = W_{fixed-wing} = 2.50$ [N]
2. $V_{\infty} = 5$ [m/s]

Knowing the free-stream velocity, V_{∞} , the coefficients of lift and drag for the fixed-wing MAV can be calculated using standard sea-level density and a wing area of $S = .258$ m^2

$$C_L = \frac{2W}{\rho V_{\infty}^2 S} = 0.634 \quad (1)$$

$$C_D = C_{D,0} + \frac{C_L^2}{\pi \lambda e} = 0.150 \quad (2)$$

where the zero-lift drag coefficient, $C_{D,0}$ was estimated to be 0.05 for extremely low Reynold's numbers ($Re < 100,000$) and a worst case span efficiency factor (i.e. rectangular wing) was chosen, $e = 0.7$ [1]. The aspect ratio is defined as $\lambda \equiv \frac{b^2}{S}$ or 1.82 (with $b = .686$ m). During cruise flight, the thrust required must equal the drag exerted on the aircraft body

$$T_{fw} = D = \frac{1}{2} \rho V_{\infty}^2 S C_D = 0.59[N] \quad (3)$$

In comparison, the thrust required for a helicopter during cruise is equal to

$$T_{heli} = \frac{W}{\cos \epsilon} = 2.50[N] \quad (4)$$

where ϵ is the angle the thrust vector makes with the vertical axis. Assuming a small ϵ , the thrust must equal the weight. Equations 3 and 4 show that the thrust required for a rotary-wing MAV is approximately more than four times that of its fixed-wing counterpart.

2.2 Endurance

With a larger thrust requirement, it can be shown that rotary-wing MAVs cannot sustain cruise flight for very long when compared with fixed-wing MAVs. In this analysis, the following assumptions were made

1. motor is the main source of current draw
2. motor-prop combo is not geared (direct drive)
3. heli battery cap = fixed-wing battery cap

The thrust generated by a propeller is given by the equation

$$T = C_T \rho A (\omega R)^2 \quad (5)$$

where C_T is the coefficient of thrust. This relationship shows that the thrust is proportional to the square of the propeller's angular velocity ($T \propto \omega^2$) or

$$\omega \propto \sqrt{T} \quad (6)$$

Furthermore, the angular velocity of a motor is proportional to the current draw ($\omega \propto I_{motor}$). And since flight time is equal to

$$E = \frac{\text{capacity}}{I_{motor}} \quad (7)$$

it holds true that $E \propto \frac{1}{I_{motor}}$. The net result is that aircraft endurance is inversely proportional to the square root of thrust

$$E \propto \frac{1}{\sqrt{T}} \quad (8)$$

Plugging in the values from equations 3 and 4, we have the following comparison for fixed-wing and rotary-wing endurance during cruise flight

$$\frac{E_{fw}}{E_{heli}} = \frac{\sqrt{T_{heli}}}{\sqrt{T_{fw}}} = 2.06 \quad (9)$$

It is evident from the equation above that a fixed-wing configuration offers a significant endurance advantage over helicopters and other rotary-wing aircraft. Conversely, the main drawback is the inability to hover. However, combining the latest advancements in battery technology and electric motors with lightweight airframes (i.e. high thrust-to-weight ratio) makes hovering a fixed-wing aircraft possible.

3 Cruise-to-Hover Transition

The addition of hovering as a secondary flight modality optimizes the fixed-wing MAV configuration. Furthermore, a quick transition from cruise to hover flight enables a failsafe maneuver to avoid a collision. Our prototype was designed to allow this transition to occur with a turning radius of less than 1 m and a 2 second response time. This allows for a plane flying directly into an obstacle at 5 m/s to avoid the collision by detecting the presence of the obstacle just 1 meter away (see Figure 2), easily achieved with a conventional proximity sensor.

The most critical aspect of this design is the transition from cruise to hover flight. During this phase,

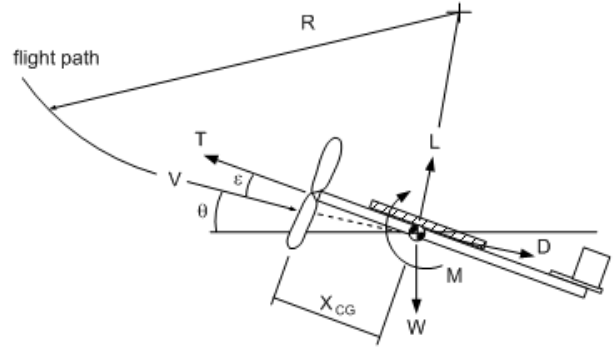


Figure 4: Free body diagram of a fixed-wing aircraft during a pitching maneuver.

there exists an angle-of-attack, α , for which the wings are no longer a contributing factor to the lift component (i.e. stall). To achieve the maneuver, the aircraft essentially has to *bully* its way through the stall regime (see Figure 3). This requires that large thrust-to-weight ratios ($T/W > 1$) be incorporated into the design. Furthermore, the aircraft must be controlled with limited airflow (i.e. prop wash) over the control surfaces once in the hovering position. As a result, the control surface areas of the horizontal and vertical tails, along with the wing must be increased. The net result is that a small wind force can be used to regulate rotation about all three axes.

3.1 Governing Dynamics

The four forces of flight acting on the aircraft during this large angle-of-attack maneuver are lift (L), weight (W), thrust (T) and drag (D) (see Figure 4). Summing the forces parallel and perpendicular to the flight path, which is opposite to the free-stream velocity, yields the following two equations

$$-D - W \sin \theta + T \cos \epsilon = m \dot{V} \quad (10)$$

$$L - W \cos \theta + T \sin \epsilon = m V \dot{\theta} \quad (11)$$

where V is the aircraft velocity tangential to the flight path, ϵ is the angle between the thrust vector and the free-stream velocity and θ is the aircraft pitch angle with respect to the horizontal. Taking the sum of the moments about the aircraft's center of gravity (CG) yields the third and final equation of motion

$$M + (T \sin \epsilon) X_{CG} = I_{CG} \ddot{\theta} \quad (12)$$

It can be seen from equation 10 (parallel to the flight path) that when the aircraft transitions to the hov-

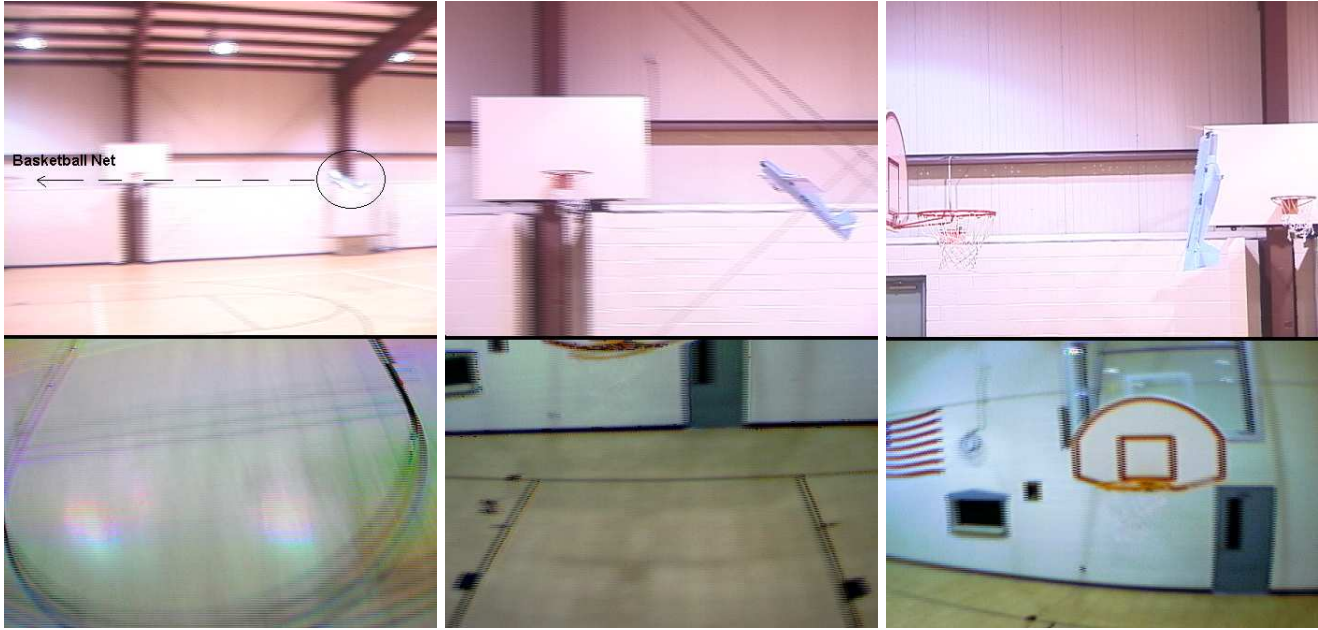


Figure 2: Under manual control, the MAV prototype avoids a collision with a basketball net through a quick transition to the secondary flight modality (top). Also, pics from the wireless camera mounted on the belly of the MAV are shown (bottom).

ering position (i.e. $\theta = 90$ and $\dot{V} = 0$), the thrust generated from the propeller (T) must balance both the aircraft weight and drag forces (assuming small ϵ). However, since the aircraft is stationary, the only drag being exerted on the airframe is a result of the prop-wash and is assumed to be small. Therefore, the thrust should be equal to the weight of the aircraft during hover.

3.2 Simulation and Flight Data

Equation 10 was modeled in Simulink (see Figure 5). The thrust was estimated with a ramp function with the upper and lower limits being equal to the aircraft weight and required thrust during cruise (from equation 3), respectively. With a turning radius of 1 meter, the aircraft reaches the hovering position in less than 2 seconds. Figure 6 shows the simulation results in terms of the aircraft pitch angle, θ , over time.

To confirm the simulation results, an infrared temperature sensor was mounted to the fuselage in order to measure the aircraft's pitch angle. The MAV was then manually piloted to conduct several cruise to hover transitions. The data was logged to a recorder mounted onboard the aircraft and three trials are shown in figure 7. The last trial run (denoted by x's) was into a strong headwind (≈ 10 mph) and thus re-

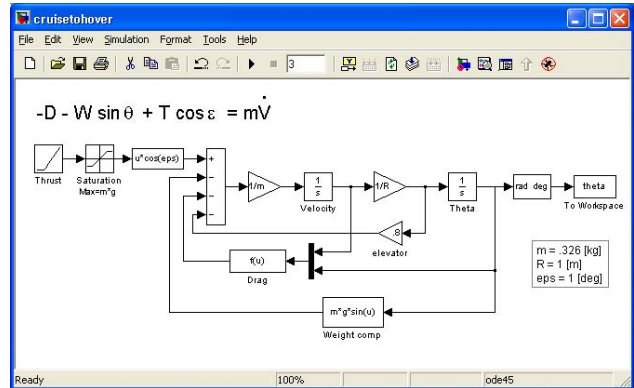


Figure 5: Equation 10 modeled in Simulink.

quired some forward thrust to remain in a stationary position. This resulted in an aircraft pitch angle of around 60 degrees in order to stabilize the MAV.

4 Future Work

Different missions will require larger payload capacities and longer flight times. As such, the authors plan to evaluate the effects of scaling the original prototype. Larger scale versions will decrease its ability to be man-portable while smaller scale versions will



Figure 3: Our MAV prototype with a 30 inch wingspan transitions from cruise flight (left) through the stall regime (middle) and into a hovering position (right).

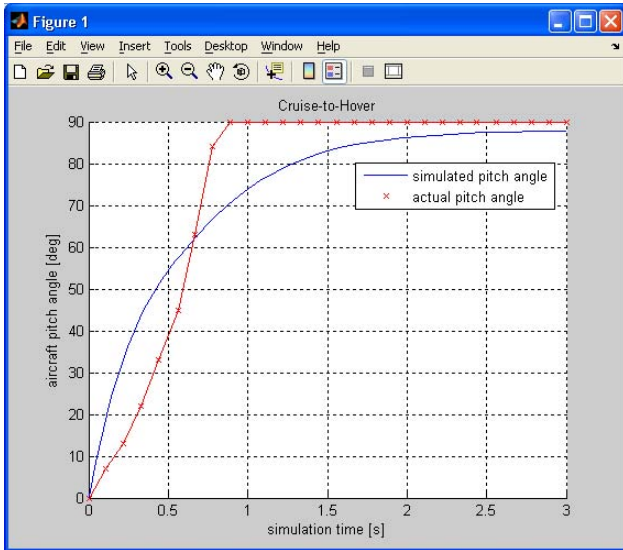


Figure 6: The simulation of an aircraft's pitch angle (smooth line) is compared with actual flight data (x's) during transition from cruise to hover. A steady-state value of 90 degrees is reached in about 2 seconds.

be restricted by payload capacities and outdoor flying conditions (e.g. wind gusts). In addition, we are currently designing a sensor suite and control system that will enable an autonomous transition from primary to secondary flight modes. For this, onboard processing is preferred because of communication limitations in near-Earth environments. This requires lightweight sensor packages such as Analog Devices' ADXRS150, a micro angular rate sensor weighing less than 3 grams. Three sensors will be interfaced, orthogonally, to measure angular rate about the roll, pitch, and yaw axes. To help correct error associated with drift, optic flow sensors will be integrated into the design of the sensor suite. Figure 8 depicts an optic flow microsensors which, including optics, imaging,

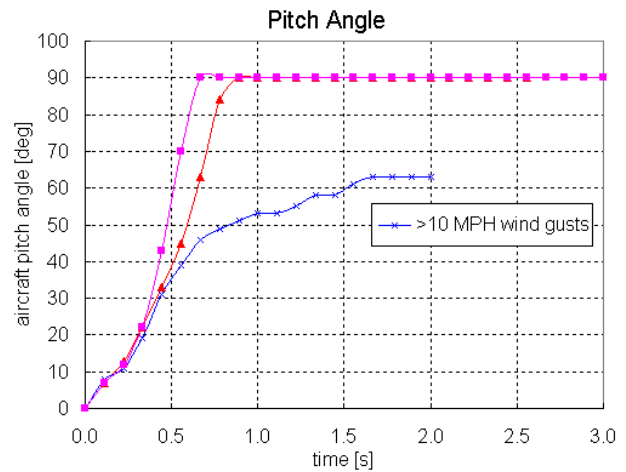


Figure 7: Actual flight data showing the MAV pitch angle reaching 90 degrees in less than 2 seconds.

processing, and I/O, weighs just 4.8 grams [2]. This analog VLSI sensor grabs frames up to 1.4 kHz, measures optic flow up to 20 rad/s (4 bit output), and functions even when texture contrast is just several percent.

In addition to providing angular rate, optic flow can also be used to gain information on incoming collisions and altitude. Figure 9 depicts optic flow as it might be seen by a MAV traveling a straight line above the ground. The focus of expansion (FOE) in the forward sensor view indicates the direction of travel. If the FOE is located inside a rapidly diverging region, then a collision is imminent. A rapidly expanding region to the right of the FOE (like the one seen in the Figure 9) corresponds to an obstacle approaching on the right side of the MAV. Mimicking insect flight stratagems [11], the MAV should turn left, or away from the region of high optic flow, to avoid the collision. Simi-

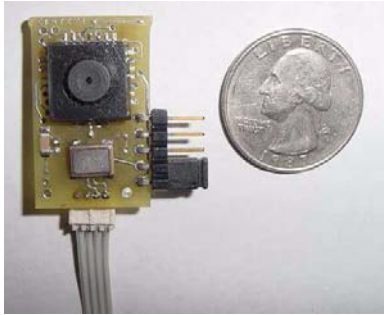


Figure 8: Centeye's optic flow sensor weighing just 4.8 grams.

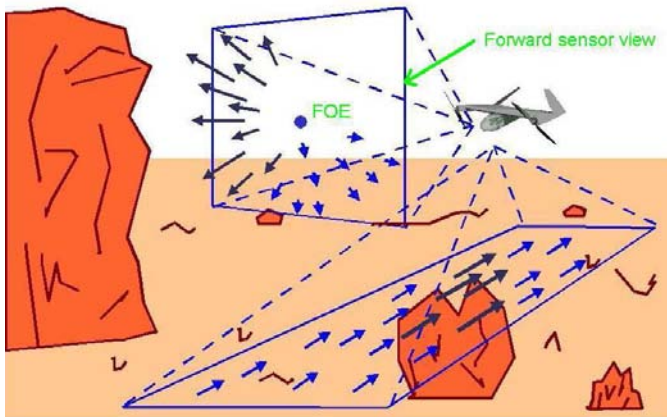


Figure 9: Optic flow as seen by MAV flying above ground.

larly, the MAV can estimate its height from the optic flow in the downward direction; faster optic flow indicates a lower altitude. These navigation strategies can be embedded into the control architecture of the sensor suite for autonomous navigation [9] [7].

5 Conclusion

Near-Earth environments are rugged and rich with obstacles. Usually enclosed or covered (e.g. forest canopy), line-of-sight to GPS satellites is occluded and communications are degraded. Furthermore, potential MAV missions, such as gathering reconnaissance around a mountain or over a hill a few miles ahead, demands high endurance traits. Such characteristics require that aerial platforms be able to fly safely and slowly for lengthy periods of time as well as unconventional approaches towards autonomous flight. The successful design of a fixed-wing MAV with hovering capabilities offers both the endurance superiority of

fixed-wing platforms along with the benefits of stationary flight. Furthermore, the small turning radius during the transition from cruise to hover flight allows for a failsafe maneuver to avoid an imminent collision. The net result is a platform which yields high endurance in its primary flight mode, but can morph to a second modality to hover or avoid a collision.

References

- [1] Anderson, J.D., *Aircraft Performance and Design*, McGraw-Hill, 1999.
- [2] Barrows, G., "Mixed-Mode VLSI Optic Flow Sensors for Micro Air Vehicles", *Ph.D. Dissertation*, University of Maryland, College Park, MD, Dec. 1999.
- [3] Choi, H., Sturdza, P., Murray, R.M., "Design and Construction of a Small Ducted Fan Engine for Non-linear Control Experiments", *Proc. American Control Conf.*, Baltimore MD, pp. 2618-2622, June 1994.
- [4] Fearing, R., et al, "Wing Transmission for a Micromechanical Flying Insect", *IEEE Int Conf Robotics and Automation*, San Francisco pp. 1509-1516, April 2000.
- [5] Grasmeyer, J.M., Keennon, M.T., "Development of the Black Widow Micro Air Vehicle", *39th AIAA Aerospace Sciences Meeting and Exhibit*, Reno, NV, Jan. 2001.
- [6] Green, W.E., Oh, P.Y., Barrows, G., "Flying Insect Inspired Vision for Autonomous Aerial Robot Maneuvers in Near-Earth Environments", *IEEE International Conference of Robotics and Automation*, pp. 2347-2352, New Orleans, LA, April 2004.
- [7] Higgins, C., "Sensory architectures for biologically-inspired autonomous robotics," *The Biological Bulletin*, vol. 200, pp 235-242, April 2001.
- [8] Hamel, T.; Mahony, R., Chriette, A., "Visual Servo Trajectory Tracking for a Four Rotor VTOL Aerial Vehicle", *IEEE International Conference on Robotics and Automation (ICRA)*, Washington, D.C., pp. 2781-2786, 2002.
- [9] Netter, T., Francheschini, N., "A Robotic Aircraft that Follows Terrain Using a Neuromorphic Eye", *IEEE/RSJ Int Conf on Intelligent Robots and Systems*, V1, pp. 129-134, Lausanne, Switz., Sept. 2002.
- [10] Oh, P.Y., Green, W.E., "Closed Quarter Aerial Robot Prototype to Fly In and Around Buildings", *Int. Conference on Computer, Communication and Control Technologies*, Vol. 5, pp. 302-307, Orlando, FL, July 2003.
- [11] Srinivasan, M.V., Chahl, J.S., Weber, K., Venkatesh, S., Nagle, M.G., Zhang, S.W., *Robot Navigation Inspired By Principles of Insect Vision in Field and Service Robotics*, A. Zelinsky (ed), Springer Verlag Berlin, NY 12-16.